Research Article | Vol. 25, No. 25 | 11 Dec 2017 | OPTICS EXPRESS 31281
Optics EXPRESS

Parametric study of high-performance 1.55 μm InAs quantum dot microdisk lasers on Si

Si Zhu,[1,2] Bei Shi,[1,2] Qiang Li,[1] Yating Wan,[1] and Kei May Lau[1,*]

[1]*Department of Electronic and Computer Engineering, Hong Kong University of Science and Technology, Clear Water Bay, Kowloon, Hong Kong*
[2]*S. Zhu and B. Shi contributed equally to this work*
[*]*eekmlau@ust.hk*

Abstract: In this paper, we present a parametric study of high performance microdisk lasers at 1.55 μm telecom wavelength, monolithically grown on on-axis (001) Si substrates incorporating quantum dots (QDs) as gain elements. In the optimized structure, seven layers of QDs were adopted to provide a high gain as well as a suppressed inhomogeneous broadening. The same laser structure employing quantum wells (QWs) on Si was concurrently evaluated, showing a higher threshold and more dispersive quantum efficiency than the QDs. Finally, a statistical comparison of these Si-based QD microdisk lasers with those grown on InP native substrates was conducted, revealing somewhat higher thresholds but of the same order. The monolithically grown QD microlasers on Si also demonstrated excellent temperature stability, with a record high characteristic temperature of 277 K. This work thus offers helpful insight towards the optimization of reliable Si-based QD lasers at 1550 nm.

OCIS codes: (140.5960) Semiconductor lasers; (140.3948) Microcavity devices; (230.5590) Quantum-well, -wire and -dot devices.

References and links

1. Z. Wang, B. Tian, M. Pantouvaki, W. Guo, P. Absil, J. Van Campenhout, C. Merckling, and D. Van Thourhout, "Room-temperature InP distributed feedback laser array directly grown on silicon," Nat. Photonics **9**, 837–842 (2015).
2. D. Liang, X. Huang, G. Kurczveil, M. Fiorentino, and R. G. Beausoleil, "Integrated finely tunable microring laser on silicon," Nat. Photonics **10**, 719–722 (2016).
3. K. Preston, P. Dong, B. Schmidt, and M. Lipson, "High-speed all-optical modulation using polycrystalline silicon microring resonators," Appl. Phys. Lett. **92**, 151104 (2008).
4. D. Feng, S. Liao, P. Dong, N. N. Feng, H. Liang, D. Zheng, C. C. Kung, J. Fong, R. Shafiiha, J. Cunningham, and A. V. Krishnamoorthy, "High-speed Ge photodetector monolithically integrated with large cross-section silicon-on-insulator waveguide," Appl. Phys. Lett. **95**, 261105 (2009).
5. S. Chen, M. Liao, M. Tang, J. Wu, M. Martin, T. Baron, A. Seeds, and H. Liu, "Electrically pumped continuous-wave 1.3 μm InAs/GaAs quantum dot lasers monolithically grown on on-axis Si (001) substrates," Opt. Express **25**(5), 4632–4639 (2017).
6. J. Yang, P. Bhattacharya, and Z. Mi, "High-performance In0.5Ga0.5As/GaAs quantum-dot lasers on silicon with multiple-layer quantum-dot dislocation filters," IEEE Trans. Electron Dev. **54**, 2849–2855 (2007).
7. B. Shi, Q. Li, and K. M. Lau, "Self-organized InAs/InAlGaAs quantum dots as dislocation filters for InP films on (001) Si," J. Cryst. Growth **464**, 28–32 (2017).
8. A. Y. Liu, S. Srinivasan, J. Norman, A. C. Gossard, and J. E. Bowers, "Quantum dot lasers for silicon photonics," Photonics Res. **3**, B1–B9 (2015).
9. S. Chen, W. Li, J. Wu, Q. Jiang, M. Tang, S. Shutts, S. N. Elliott, A. Sobiesierski, A. J. Seeds, I. Ross, P. M. Smowton, and H. Liu, "Electrically pumped continuous-wave III–V quantum dot lasers on silicon," Nat. Photonics **10**, 307–311 (2016).
10. A. Y. Liu, C. Zhang, J. Norman, A. Snyder, D. Lubyshev, J. M. Fastenau, A. W. K. Liu, A. C. Gossard, and J. E. Bowers, "High performance continuous wave 1.3 μm quantum dot lasers on silicon," Appl. Phys. Lett. **104**, 041104 (2014).
11. M. Z. M. Khan, T. K. Ng, and B. S. Ooi, "Self-assembled InAs/InP quantum dots and quantum dashes: Material structures and devices," Prog. Quantum Electron. **38**, 237–313 (2014).
12. B. Shi, S. Zhu, Q. Li, C. W. Tang, Y. Wan, E. L. Hu, and K. M. Lau, "1.55 μm room-temperature lasing from subwavelength quantum-dot microdisks directly grown on (001) Si," Appl. Phys. Lett. **110**, 121109 (2017).

#308539 https://doi.org/10.1364/OE.25.031281
Journal © 2017 Received 6 Oct 2017; revised 19 Nov 2017; accepted 27 Nov 2017; published 30 Nov 2017

13. M. Liao, S. Chen, S. Hou, S. Chen, J. Wu, M. Tang, K. Kennedy, W. Li, S. Kumar, M. Martin, T. Baron, C. Jin, I. Ross, A. Seeds, and H. Liu, "Monolithically integrated electrically pumped continuous-wave III-V quantum dot light sources on silicon," IEEE J. Sel. Top. Quantum Electron. **23**, 1900910 (2017).
14. K. Volz, A. Beyer, W. Witte, J. Ohlmann, I. Németh, B. Kunert, and W. Stolz, "GaP-nucleation on exact Si (001) substrates for III/V device integration," J. Cryst. Growth **315**, 37–47 (2011).
15. Y. Gao, Z. Zhong, S. Feng, Y. Geng, H. Liang, A. W. Poon, and K. M. Lau, "High-speed normal-incidence pin InGaAs photodetectors grown on silicon substrates by MOCVD," IEEE Photonics Technol. Lett. **24**, 237–239 (2012).
16. Y. Geng, S. Feng, A. W. Poon, and K. M. Lau, "High-speed InGaAs photodetectors by selective-area MOCVD toward optoelectronic integrated circuits," IEEE J. Sel. Top. Quantum Electron. **20**, 36–42 (2014).
17. Q. Li, X. Zhou, C. W. Tang, and K. M. Lau, "Material and Device Characteristics of Metamorphic $In_{0.53}Ga_{0.47}As$ MOSHEMTs Grown on GaAs and Si Substrates by MOCVD," IEEE Trans. Electron Dev. **60**, 4112–4118 (2013).
18. R. Nagarajan, M. Kato, J. Pleumeekers, P. Evans, S. Corzine, S. Hurtt, A. Dentai, S. Murthy, M. Missey, R. Muthiah, R. A. Salvatore, C. Joyner, R. Schneider, J. M. Ziari, F. Kish, and D. Welch, "InP photonic integrated circuits," IEEE J. Sel. Top. Quantum Electron. **16**, 1113–1125 (2010).
19. B. Shi, S. Zhu, Q. Li, Y. Wan, E. L. Hu, and K. M. Lau, "Continuous-wave optically pumped 1.55 μm InAs/InAlGaAs quantum dot microdisk lasers epitaxially grown on silicon," ACS Photonics **4**, 204–210 (2017).
20. S. L. McCall, A. F. J. Levi, R. E. Slusher, S. J. Pearton, and R. A. Logan, "Whispering-gallery mode microdisk lasers," Appl. Phys. Lett. **60**, 289–291 (1992).
21. D. Y. Chu, M. K. Chin, N. J. Sauer, Z. Xu, T. Y. Chang, and S. T. Ho, "1.5 μm InGaAs/InAlGaAs quantum-well microdisk lasers," IEEE Photonics Technol. Lett. **5**, 1353–1355 (1993).
22. R. Nötzel, S. Anantathanasarn, R. P. Van Veldhoven, F. W. Van Otten, T. J. Eijkemans, and A. Trampert, "Self-assembled InAs/InP quantum dots for telecom applications in the 1.55 μm wavelength range: wavelength tuning, stacking, polarization control, and lasing," Jpn. J. Appl. Phys. **45**, 6544 (2006).
23. M. Lipinski, H. Schuler, O. Schmidt, K. Eberl, and N. Jin-Phillipp, "Strain-induced material intermixing of InAs quantum dots in GaAs," Appl. Phys. Lett. **77**, 1789–1791 (2000).
24. I. Aharonovich, A. Woolf, K. J. Russell, T. Zhu, N. Niu, M. J. Kappers, R. A. Oliver, and E. L. Hu, "Low threshold, room-temperature microdisk lasers in the blue spectral range," Appl. Phys. Lett. **103**, 021112 (2013).
25. D. Lacombe, A. Ponchet, J. M. Gérard, and O. Cabrol, "Structural study of InAs quantum boxes grown by molecular beam epitaxy on a (001) GaAs-on-Si substrate," Appl. Phys. Lett. **70**, 2398–2400 (1997).
26. S. Zhu, B. Shi, Y. Wan, E. L. Hu, and K. M. Lau, "1.55 μm band low-threshold, continuous-wave lasing from InAs/InAlGaAs quantum dot microdisks," Opt. Lett. **42**(4), 679–682 (2017).
27. S. Chen, M. Tang, Q. Jiang, J. Wu, V. G. Dorogan, M. Benamara, Y. I. Mazur, G. J. Salamo, P. Smowton, A. Seeds, and H. Liu, "InAs/GaAs quantum-dot superluminescent light-emitting diode monolithically grown on a Si substrate," ACS Photonics **1**, 638–642 (2014).
28. Ž. Gačević, A. Das, J. Teubert, Y. Kotsar, P. K. Kandaswamy, T. Kehagias, T. Koukoula, Ph. Komninou, and E. Monroy, "Internal quantum efficiency of III-nitride quantum dot superlattices grown by plasma-assisted molecular-beam epitaxy," J. Appl. Phys. **109**, 103501 (2011).
29. F. Klopf, J. P. Reithmaier, and A. Forchel, "Highly efficient GaInAs/(Al) GaAs quantum-dot lasers based on a single active layer versus 980 nm high-power quantum-well lasers," Appl. Phys. Lett. **77**, 1419–1421 (2000).
30. G. T. Liu, A. Stintz, H. Li, T. C. Newell, A. L. Gray, P. M. Varangis, K. J. Malloy, and L. F. Lester, "The Influence of Quantum-Well Composition on the Performance of Quantum Dot Lasers Using InAs/InGaAs Dots-in-a-Well (DWELL) Structures," IEEE J. Quantum Electron. **36**, 1272–1279 (2000).
31. H. A. R. El-Ella, F. Rol, M. J. Kappers, K. J. Russell, E. L. Hu, and R. A. Oliver, "Dislocation density-dependent quality factors in InGaN quantum dot containing microdisks," Appl. Phys. Lett. **98**, 131909 (2011).
32. J. Tatebayashi, S. Kako, J. Ho, Y. Ota, S. Iwamoto, and Y. Arakawa, "Room-temperature lasing in a single nanowire with quantum dots," Nat. Photonics **9**, 501–505 (2015).
33. Y. Wan, Q. Li, A. Y. Liu, A. C. Gossard, J. E. Bowers, E. L. Hu, and K. M. Lau, "Temperature characteristics of epitaxially grown InAs quantum dot micro-disk lasers on silicon for on-chip light sources," Appl. Phys. Lett. **109**, 011104 (2016).
34. J. Van Campenhout, P. Rojo-Romeo, D. Van Thourhout, C. Seassal, P. Regreny, L. Di Cioccio, F. Jean-Marc, and R. Baets, "Thermal characterization of electrically injected thin-film InGaAsP microdisk lasers on Si," J. Lightwave Technol. **25**, 1543–1548 (2007).
35. T. Ide, T. Baba, J. Tatebayashi, S. Iwamoto, T. Nakaoka, and Y. Arakawa, "Room temperature continuous wave lasing in InAs quantum-dot microdisks with air cladding," Opt. Express **13**(5), 1615–1620 (2005).
36. M. Wu, Y. Chen, J. Kuo, M. Chin, and A. Sergent, "High temperature, high power InGaAs/GaAs quantum-well lasers with lattice-matched InGaP cladding layers," IEEE Photonics Technol. Lett. **4**, 676–679 (1992).
37. Y. P. Varshni, "Temperature dependence of the energy gap in semiconductors," Physica **34**(1), 149–154 (1967).
38. Z. M. Fang, K. Y. Ma, D. H. Jaw, R. M. Cohen, and G. B. Stringfellow, "Photoluminescence of InSb, InAs, and InAsSb grown by organometallic vapor phase epitaxy," J. Appl. Phys. **67**, 7034 (1990).
39. R. Debusmann, T. W. Schlereth, S. Gerhard, W. Kaiser, S. Höfling, and A. Forchel, "Gain Studies on Quantum-Dot Lasers With Temperature-Stable Emission Wavelength," IEEE J. Quantum Electron. **44**, 175 (2008).

Optics EXPRESS

1. Introduction

With high efficiency and high speed operation due to their high quality factor Q and small volume V, microdisk lasers (MDLs) emitting at near infrared wavelengths are excellent candidates for on-chip integration. A more strategic approach is to heterogeneously integrate these advanced small lasers on a silicon platform to benefit from the well-developed CMOS technologies. To fully exploit the massive scalable integration and extremely low-cost features of the Si manufacturing platform, Si-based photonic integrated circuits (PICs) leveraging optical interconnects are booming to accommodate the exponentially growing requests for telecommunications and big data processing [1, 2]. Tremendous progress has been made in Group IV-based light modulation and detection devices [3, 4]. However, as the most vital component in the PICs, on-chip laser source remains a challenge. The monolithic growth method to integrate III-V lasers on Si has gained renewed interest and been extensively investigated in recent years by virtue of the potential low-cost, high-yield, and large-scale integration of complex optoelectronic circuits [5]. Nevertheless, fundamental challenges including high density (10^9-10^{10} cm^{-2}) of threading dislocations (TDs) and planar defects associated with material mismatch and different polarities of III-V and Si are impeding the advancement of heteroepitaxy. The emergence of quantum dots (QDs) as a superior gain material, is ideal for the development of the direct epitaxy of lasers on silicon. The large strain field of QDs can propel or pin the dislocations originated from the bottom hetero-interface of III-V and Si to form dislocation loops [6, 7]. Moreover, the spatially discrete nature of these dense three-dimensional nanostructures alleviates the influence of defects, outperforming the conventional quantum wells [8]. To date, excellent injection QD lasers on Si have been demonstrated with low threshold current density, high operation temperature and long lifetime [9, 10]. Yet the longest emission wavelength reported for such lasers is 1.3 μm, utilizing InAs/GaAs QDs, and for the important C-band lasers at 1.55 μm, progress is hindered by two factors: first, difficulties in achieving uniform and dense InAs QDs on InP due to the small lattice mismatch (only ~3.2%) and complex strain distribution [11], and second, challenges in InP-on-Si buffer growth with a quite large lattice mismatch of ~8% [7].

Recently, our group demonstrated the first room-temperature lasing of 1.55 μm QD lasers directly grown on (001) Si [12]. In the present paper, further investigation into the influential parameters of 1.55 μm QD microdisk lasers on silicon has been conducted, focusing on: 1) the impact of active membrane thickness; 2) a comparison with quantum well microdisk lasers; 3) statistical benchmarking with devices grown on InP native substrates and finally, 4) temperature properties of the QD lasers on Si with a record high characteristic temperature. This analysis offers insights into optimized long-wavelength lasers on Si substrates.

2. Experimental methods

The material growth was started on a standard 4-inch nominal (001) silicon substrate. After an RCA-1 cleaning process and 1% diluted HF solution dip for 1 min, the prepared Si substrate was loaded into an Aixtron 200/4 horizontal reactor metal-organic chemical vapor deposition (MOCVD) system for epitaxial growth. The growth details for InP-on-Si template were described elsewhere [12]. The microdisk membrane was grown on the InP buffer, with seven layers of InAs/In(Al)GaAs dot-in-wells (DWELLs) cladded in symmetrical InAlAs layers. The whole epi-structure is illustrated in Fig. 1(a). The III-V on silicon structures employed here eliminate the utilization of either patterned Si substrates that require nano-pattern lithography and etching processes [13], or specialized offcut Si wafers not commonly used in CMOS fabs and cost-intensive [14]. Our developed InP-on-Si (IoS) template technology can ease the transfer of incumbent InP-based optoelectronic devices and PIC technologies onto the advanced Si manufacturing platform [15–18], contributing to future dense optoelectronic integration and high speed data communications. The same device structure was also grown on InP substrates for benchmarking.

The as-grown materials on InP and IoS substrates were processed into MDLs with a diameter of 4 μm by combining colloidal lithography with a two-step etching method [19], as shown in Fig. 1(b). More specifically, 4-μm-diameter silica microbeads diluted in isopropyl alcohol (IPA) solutions were dispersed onto the as-grown samples with 200 nm SiO_2 deposited as the hard mask, by plasma-enhanced chemical vapor deposition (PECVD). Reactive ion etching (RIE) was then performed to transfer the perfectly round patterns down through the oxide. This "double-mask" approach can result in a smooth and steep sidewall of the microdisks, while keeping the top InAlAs cladding undamaged. Inductively coupled plasma (ICP) dry etching was conducted subsequently, with the etching depth targeted at over 1 μm. Afterwards, the microspheres were removed by acetone in an ultrasonic bath, and the InP pedestal was formed by immersing the sample in a 50% diluted HCl solution for 90 s to form a mushroom-shaped structure. Coupling of the air-cladded whispering-gallery modes (WGMs) near the periphery of the disk to the buffer/substrates is minimized. Figure 1(c) shows a 70° tilted scanning electron microscope (SEM) image of a fabricated device on Si, revealing a vertical and smooth sidewall.

For the optical characterization of the as-grown samples, room-temperature macro-photoluminescence (RT-PL) was conducted, while for the MDLs measurement, power and temperature dependent micro-photoluminescence (μPL) was performed, pumped by a pulsed laser source (532 nm, 20 ns pulse width and 3 kHz repetition rate). The laser spot was focused to a diameter of 4 μm, matching the size of microdisk lasers. It should be noted that the pump power referred here is the average power of the pulsed laser.

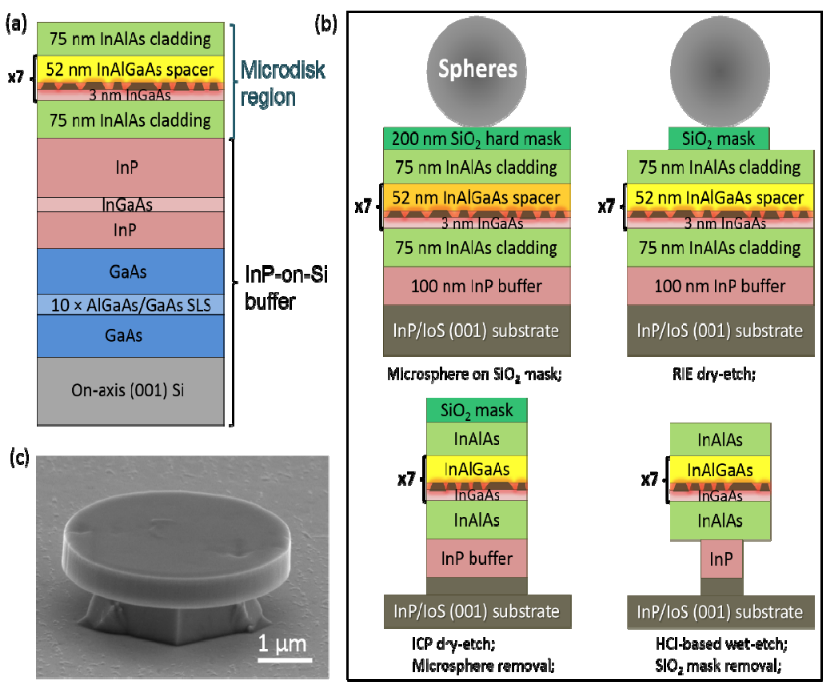

Fig. 1. (a) Schematic diagram of the microdisk laser structure on Si substrate; (b) processing steps in the microdisk laser fabrication; (c) 70° tilted SEM image of the fabricated device on Si, revealing a smooth and steep sidewall topology.

Optics EXPRESS

3. Results and discussion

3.1 Microdisk membrane thickness

In this study, we investigated the influence of the microdisk membrane thickness on the laser threshold with two different active laser structures. In principle, a thinner disk with fewer stacks of QDs can potentially offer a lower threshold due to a smaller active volume, together with a suppression of higher order modes in the longitudinal direction [20]. The cutoff thickness for the second-order waveguide mode is $h_c = \lambda_0 / 2n_d$ [21], where λ_0 is referred to the emission wavelength (~1550 nm) and n_d is the refractive index of the disk membrane. Adopting the effective refractive index of the disk region as $n_d = n_{eff} = 3.4$, the calculated thickness h_c is around 230 nm. Experimentally, we also found that equipping more stacks of QDs to achieve a higher gain overcoming the loss of higher order modes in the WGM cavity is essential. However, it can be anticipated that the gain of single sheet of QDs is not sufficient to overcome the losses, while too many QD stacks (over 7 layers) may worsen the optical performance of the multiple QDs since more defective clusters will start to appear as the stack number increases, especially on Si substrates [12]. Therefore, to find out the critical QD stack numbers that can lead to the lowest power consumption, two MDL structures were carried out on InP substrates with 3 and 7 layers of QDs, resulting in different membrane thicknesses of 330 nm and 550 nm respectively. The spacing between adjacent QDs has been fixed at an optimized thickness of 53 nm for a good separation. Although the thickness for 3-layer QD MDL is somewhat larger than the calculated cutoff thickness, the influence of higher order vertical modes is minimized compared with the much thicker 7-layer QD disk.

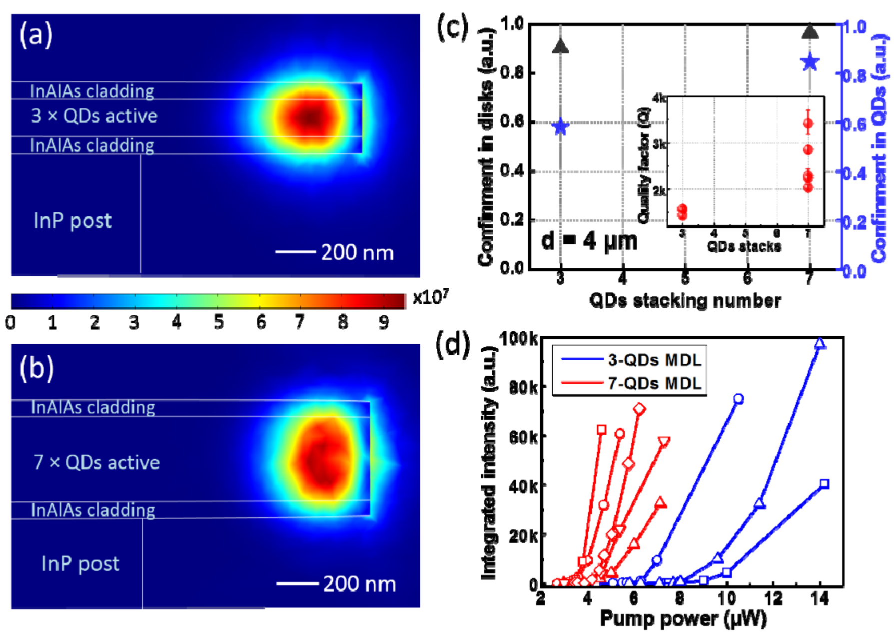

Fig. 2. (a) Cross-sectional slice of the simulated whispering gallery modes of 2D microdisks with 3-layer and (b) 7-layer QDs. (c) Calculated confinement factor of the modes inside the disk and QDs respectively. The inset demonstrates the derived cold cavity quality factors for both devices. (d) Extracted L-L curves for several microdisk lasers with 3-layer and 7-layer QDs on InP. Different symbols represents individual devices.

Figures 2(a) and 2(b) show the axial view of the simulated devices. Only the fundamental radial TE modes in this longitudinal direction were considered. The confinement factors of the disk membranes, with and without the claddings, are plotted in Fig. 2(c). It is noted that although most of the optical fields are confined inside both 3-layer QDs and 7-layer QDs disks, the effective modes that can interact with the QDs active medium is 58% for 3-layer QDs, while 85% for 7-layer QDs. In addition, the active layer gain of both MDLs, determined by room temperature PL measurements, are shown in Fig. 3, where the peak intensity for 7-QDs is about two times stronger, with a narrower full-width at half-maximum (FWHM) of only 54 meV. This indicates a more uniform QDs morphology with a larger QD stack number on the InP substrate. The intensity difference under high power excitation is further enhanced due to an increase in total active volume with more QDs stacks. The 45 nm blue-shift of the ground-state (GS) emission for the 7-QD sample can be attributed to the transition of dot-like to dash-like shape in the higher stack of QDs [22] and the strain driven material intermixing [23]. Furthermore, the quality factor *Q* of the lasing modes from microdisks with a thicker membrane is simulated to be higher than that with a thinner membrane [24]. This trend agrees well with our experimental results, where the extracted Q values are shown in the inset of Fig. 2(c). The average Q values are 2561 and 1516 for the 7-layer and 3-layer QD MDLs, respectively. These combined factors contribute to the observed lower thresholds of the 7-layer QD MDLs, as seen from the extracted output-input (L-L) curves in Fig. 2(d). In addition to the larger slope efficiency for the 7-layer QD MDL, the average threshold power of 4 μW is half of that for 3-layer QD MDLs (7.9 μW). Therefore, for the devices on Si substrate to be further explored, we chose the 7-layer QDs as the active medium, despite the total disk thickness far exceeds the calculated cutoff thickness for higher order modes of the cavity.

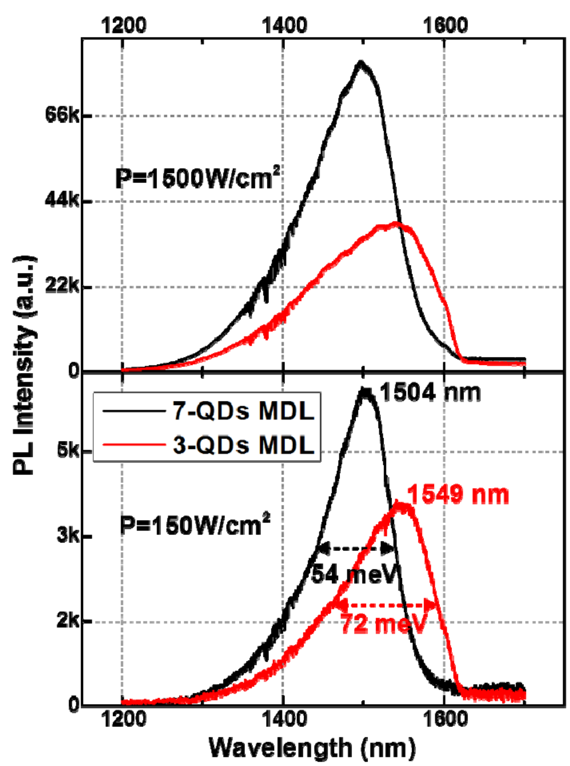

Fig. 3. Room-temperature PL comparison of as-grown samples under two different power regimes.

3.2 QD vs. QW microdisk lasers on silicon

In this section, microdisk lasers grown on silicon with an active region containing 7 layers of InAs/InAlGaAs QDs or 7 layers of InGaAs/InAlGaAs QWs are compared and discussed. It is expected that the performance of two-dimensional (2D) QWs may experience a drastic degradation when crossing dislocations generated in heteroepitaxy [8]. However, in 3D QDs, carriers can be effectively trapped and their annihilation by non-radiative recombination centers will be minimized [25]. To compare the influence of defects on these two active media, particularly threading dislocations, we firstly grew two PL structures containing only 7 layers of QWs or QDs without additional InAlAs claddings.

The room-temperature macro-PL spectra of the QWs and QDs on InP and InP-on-Si templates are displayed in Figs. 4(a) and 4(b), respectively. The dislocation density that terminated at the InP buffer top surface is in the order of 10^8/cm^2, as revealed by plan-view transmission electron microscopy (TEM). Here we pumped the structures in a low laser power regime (12.5W/cm^2), in which the defects are far from being saturated with the carriers and the PL intensity is more sensitive to distinguish the impact of dislocations on the two active materials. Compared with the same active structure grown on InP substrates, the QW sample exhibit a more severe intensity deficit on the InP-on-Si template (~12 times) than the 7-layer QDs (~6 times). Normalized spectra are shown in the inset of Figs. 4(a) and 4(b) for an evaluation of the FWHMs. For the samples grown on InP, the FWHMs are 63 meV for the 7-layer QDs and 50 meV for the 7-layer QWs, respectively. The relatively larger linewidth of the QD ensembles is due to the inhomogeneous broadening, which is associated with QDs non-uniformity [26]. The QWs on Si shows essentially the same FWHM (56 meV) as that on InP, while the FWHM of QDs on Si is enlarged to ~85 meV. This is mainly caused by the bumpy growth front of the InP buffer beneath. The broad emission spectra of QDs on Si also suggest their potential applications in superluminescent diodes [27].

Figure 4(c) plots L-L curves of several randomly selected 4-μm-diameter QD and QW microdisk lasers on silicon for a straightforward comparison. Under pulsed optical pumping, MDLs with QD and QW active layers both lase at room temperature. Nonetheless, it is obvious that the lasing thresholds of QD MDLs, clustering around 10μW, are much lower than those of the QW MDLs (25-30 μW). Furthermore, the slope efficiencies of QD lasers present a more uniform distribution across the whole sample than those of QW lasers. Both outcomes can be attributed to a higher internal quantum efficiency (IQE) and lower non-radiative recombination rate due to a stronger carrier localization in the 3D QDs structure, which has been proven in the III-nitride material system [28]. However, in QWs, carriers are much easier to diffuse toward the non-radiative recombination centers, particularly dislocations generated from the III-V/Si interface and surface of the micro-disk, resulting in a higher lasing threshold and more dispersive external quantum efficiencies. Although the 7-layer QW lasers that resulted in higher thresholds and lower efficiencies than the QD lasers might not be the optimized QW laser structure as small number of QW layer may lead to lower thresholds, we chose laser structures with the same number of active layers (QW and QD) for comparison purpose here. Lower thresholds and higher efficiencies of QD lasers on III-V substrates have been extensively verified both numerically and experimentally, comparing to its QW counterpart [29, 30]. Substituting QD active regions in place of QWs on highly mismatched silicon substrate presumably will further mitigate the negative effect of residual dislocations on laser performance, resulting in a larger difference in threshold and reliability of QD and QW lasers than those on III-V substrate.

All these results support the concept that quantum dot is a more competitive candidate than the quantum well to be used as the gain medium of lasers for monolithic integration of III-V lasers on silicon.

Optics EXPRESS

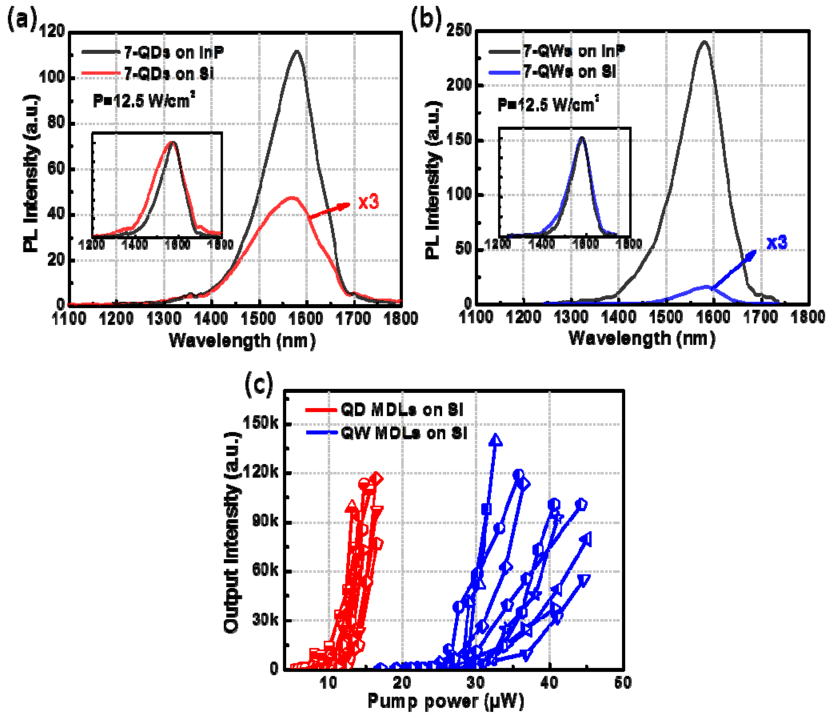

Fig. 4. Room temperature photoluminescence of the as-grown 7-layer (a) QDs and (b) QWs on InP and (001) silicon substrates. Inset: Normalized PL spectra to clearly compare the linewidths. L-L curves of MDLs on silicon substrate with (c) 7-layer QDs and QWs active medium, individual device are differentiated with different symbols.

3.3 QD microdisk lasers on Si vs. on InP substrates

To objectively compare the device performances on InP and IoS templates, the microdisk laser epitaxy was completed in the same growth run with the two substrates placed side-by-side on the satellite of the MOCVD reactor. Having undergone the same fabrication process, representative room-temperature lasing spectra of 4 μm-in-diameter MDLs on InP and IoS are exhibited in Figs. 5(a) and 5(b), respectively. The broader gain spectrum on Si (as shown in the background of Fig. 6(b) interacts with adjacent azimuthal order WGMs in the first radial order, leading to a second lasing peak with a free spectral range (FSR = $\lambda^2 / 2\pi r n_g$) of 54 nm. Generally, for both devices, when the pumping power approaches the threshold, the oscillating WGMs peak up with increasing intensity monotonically. Based on the power-dependent spectra measurement, the L-L curves as well as linewidth evolution are shown in the insets of Figs. 5(a) and 5(b). In addition to the lower threshold power for lasers on InP substrates, the cold cavity Q value (λ/△λ at transparency) for MDLs on InP is double the value of those on Si (shown in the insets of Figs. 5(a) and 5(b), extracted from two typical devices on InP and Si respectively). The lower Q value on Si is mainly attributed to a higher radiative loss and internal absorption caused by the rough InP buffer on Si, resulting in high dislocation densities inside the microdisks [31]. Abrupt linewidth reduction around the threshold region indicates a transition from spontaneous emission to lasing operation. The slight increase in linewidth well above threshold is due to the chirping effect, associated with the refractive index change resulting from the transient increase in carrier density [32].

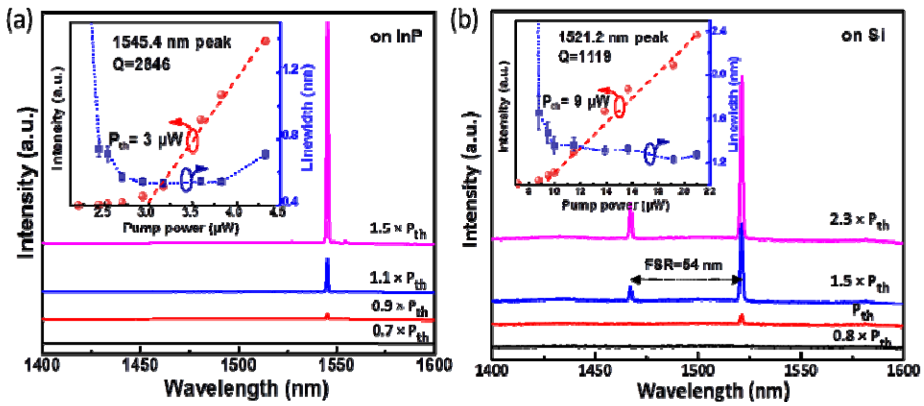

Fig. 5. Power-dependent lasing spectra of microdisks on (a) InP and (b) Si. Insets: Extracted output integrated intensity and linewidth evolution as a function of injection power. The kinks in the L-L curves signify lasing oscillation and an evident linewidth reduction occurs around the threshold regions.

Comparing typical L-L curves of the laser in Fig. 6(a), the external differential quantum efficiency of the MDL on InP is somewhat higher than that on Si. This is mainly attributed to the difference in the IQE of QDs grown on InP and Si, since the cavity loss α_{cavity} can be considered approximately the same for both structures. A statistical analysis of lasing thresholds as a function of emission wavelength is summarized in Fig. 6(b). The dispersion of lasing central wavelength of the measured samples is caused by the distribution of QDs density and their varied overlap with different radial and azimuthal order optical modes. The red and blue horizontal lines represent the average thresholds of lasers grown on Si and InP. Notably, the overall lasing thresholds on Si are somewhat higher than devices on native InP substrates, but in the same order of magnitude. This illuminates a promising path towards high performance practical injection QD lasers on Si.

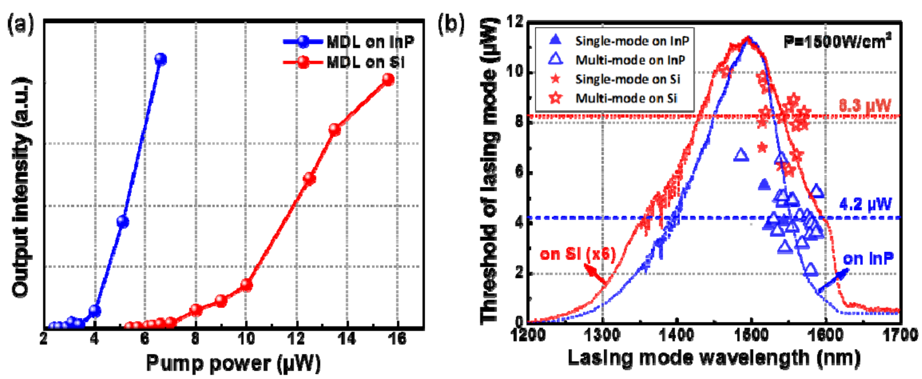

Fig. 6. (a) Representative L-L curves for microdisk lasers on InP and Si. (b) Statistical distribution of lasing thresholds. The solid symbols represent single mode lasing thresholds while the open symbols show multi-mode lasers. The background is overlaid with normalized room-temperature PL curves for samples on InP and Si. Note that the spectrum on Si has been magnified by 6 times.

The dotted lines in the background of Fig. 6(b) reveal the normalized PL curves of the as-grown materials on different substrates. As discussed above, the broader gain spectrum on Si reflects a more severe inhomogeneous broadening induced by QDs size dispersion. A smoother InP buffer is thus expected to achieve a more uniform QD morphology. Meanwhile,

Optics EXPRESS

lasing modes are observed on the lower energy side of the PL spectra, due to the reabsorption of the high-energy photons and a stronger capture efficiency of larger QDs [12].

3.4 Temperature properties of microdisk laser on Si

To evaluate the temperature characteristics of these QD MDLs, we performed μPL measurements for lasers on Si with temperatures varying from 10 K to 330 K. The maximum operating temperature of 60 °C was limited by the thermostat. Yet it is convincing that the devices are able to operate at even higher temperatures according to the normal unsaturated L-L curve at 60 °C. The capability of operation at high temperatures promises their potential applications in Si-based optoelectronic chips [2]. Figure 7(a) shows a set of normalized lasing spectra with incident power around 1.5 times of the thresholds. At lower temperatures from 10 K to 100 K, single mode lasing at a shorter wavelength occurs because of a large blue-shift of the gain spectrum at low temperatures, while another mode at longer wavelength becomes prominent when temperature rises, due to the red-shift of material gain. The mode spacing equals to the FSR equivalent to the two first-radial-order WGMs with adjacent azimuthal orders. As temperature further increases above 200 K, the mode at longer wavelength becomes stronger and finally dominates the lasing emission. Figure 7(b) plots the normalized temperature-dependent L-L curves to calculate the characteristic temperature T_0 of microdisk lasers on Si. The lasing thresholds are derived from fitting the linear region above those distinct kinks that represent the onset of lasing. As shown in Fig. 7(c), the T_0 is fitted to be 277 K in the temperature range of 150 K to 330 K, which outperforms any other reported III-V based microdisk lasers [26, 33–35]. This is a result of strong carrier confinement by the QDs and the improved material quality by optimizing the QDs on Si substrates. This T_0 value is also superior to our previous reported sub-wavelength MDLs [12]. The increase in T_0 value is because smaller disks have higher threshold gain and higher carrier concentrations at threshold, leading to carrier overflow out of the active layers [36]. Moreover, the large microdisks are less sensitive to the radiative loss and surface recombination. In addition to lasing thresholds increase, the slope efficiency is also found to degrade accordingly with temperature increment in Fig. 7(c). This can be explained by the enhanced non-radiative recombination process with decreased IQE of the active layers.

Optics EXPRESS

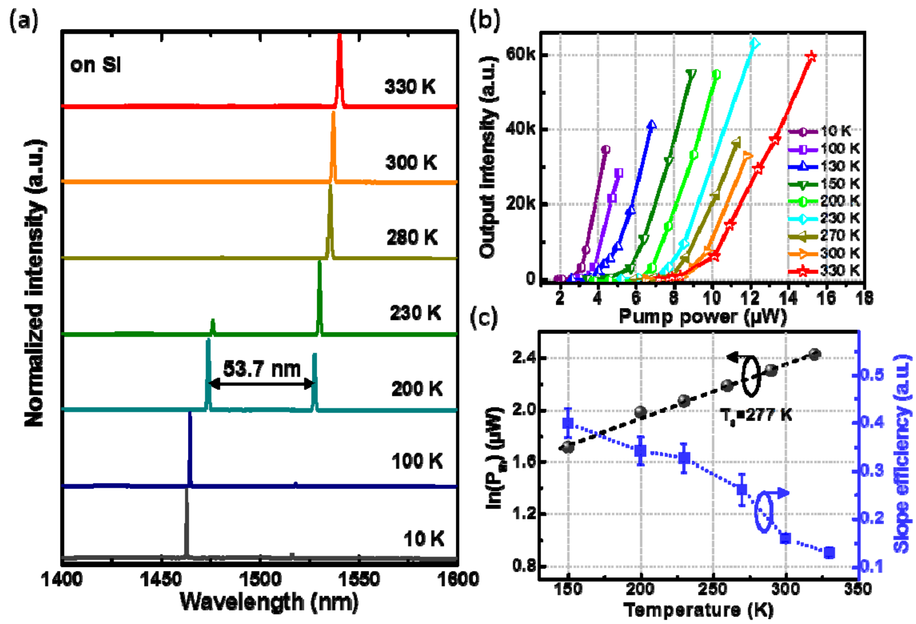

Fig. 7. (a) Normalized lasing spectra at various temperatures, ranging from 10 K to 330 K. (b) L-L curves of the lasing peaks as a function of temperature. (c) Natural logarithm of threshold powers and slope efficiencies against temperature. The characteristic temperature T_0 is fitted to be 277 K.

It is also observed that both lasing modes are red-shifted with a rate of 0.087 nm/K, which is related to refractive index change of the microdisk region, and the bandgap shrinkage of InAs QDs as temperature rises. The temperature-dependent bandgap energy is phenomenologically described by the Varshni's formula, $E_g = E_{g_0} - \frac{\alpha T^2}{T+\beta}$, where E_{g_0} is the bandgap at 0 K, α and β are two empirical parameters [37]. Figure 8 depicts the energy variation as a function of temperature for InAs/$In_{0.51}Al_{0.29}Ga_{0.2}As$ QDs. The experimental data can be well fitted with $\alpha = 0.101$ meV/K and $\beta = 518.3$ K. The lasing energy transition at 200 K is caused by mode hopping as discussed. The bandgap energy change of bulk InAs is also plotted in Fig. 8 for an intuitionistic comparison. The E_{g_0} α, and β parameters for bulk InAs are obtained from Ref [38]. It's noted that the temperature evolution of the ground state transition energy for InAs/$In_{0.51}Al_{0.29}Ga_{0.2}As$ QDs falls in between the bulk InAs and $In_{0.51}Al_{0.29}Ga_{0.2}As$ bandgaps, which are expected to be the limiting behavior for large and small QDs, respectively. Furthermore, a reduced temperature sensitivity of the emission wavelength for InAs QDs can be clearly observed. This feature of enhanced temperature stability of wavelength has also been extensively observed in InAs/(Al)GaAs QD lasers [39], which was attributed to a rather flat gain profile of a quantum dot layer.

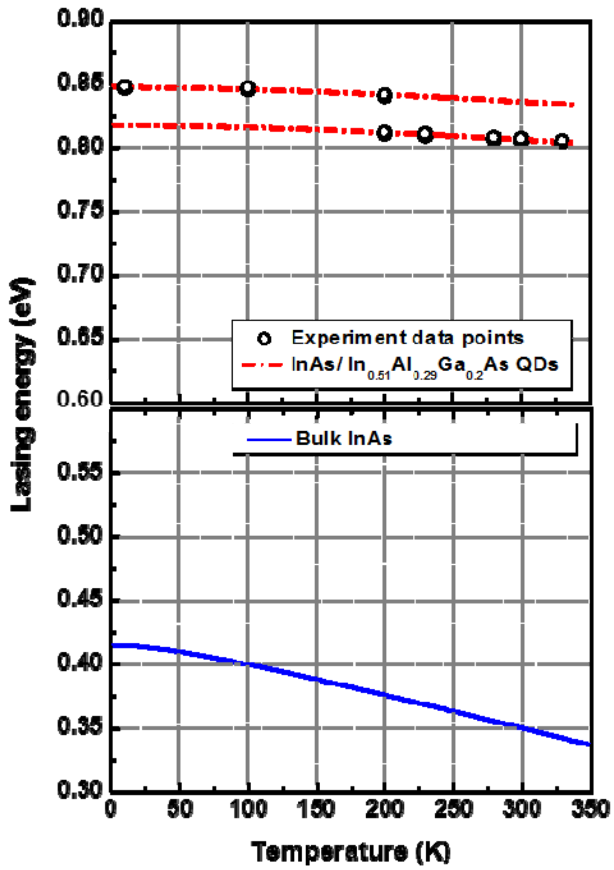

Fig. 8. Temperature-dependent lasing energy of InAs/InAlGaAs QD MDLs on silicon. The two parallel dashed red lines are fitted curves of data points extracted from Fig. 7(a), using the Varshni's formula. The blue solid line plots the bandgap change with temperature of bulk InAs.

4. Conclusion

In conclusion, we have performed a parametric analysis of 1.55 µm optically pumped quantum dot microlasers epitaxially grown on nominal Si (001) substrates. To gain some insight on the device design towards lower threshold and minimized power consumption on Si substrates, the microdisk incorporating two different QD stack numbers were fabricated and compared. An obvious lower threshold together with a higher cold cavity quality factor were achieved with 7-layer QD microdisks, due to a stronger material gain as well as a better overlap of the optical fields with the active elements. Meanwhile, a direct comparison of QDs and QWs as the gain medium in the same laser structure was performed. A lower lasing threshold and a more uniform slope efficiency distribution of QD lasers could be identified, owing to the lower sensitivity of the QDs to defects and surface recombination. Moreover, these quantum dot microdisk lasers on Si compare favorably with the devices simultaneously processed on native InP substrates, with an ultralow average threshold of 8.3 µW, a remarkable temperature stability of T_0 = 277 K and red-shift rate = 0.087 nm/K, and the capability of working at chip temperatures over 60 °C. All these results represent an advance towards reliable silicon-based quantum dot lasers at telecom wavelengths. Investigation of electrically injected QD lasers is ongoing to attain efficient and applicable light sources for on-chip photonic circuits and optical fiber communications.

Optics EXPRESS

Funding

Research Grants Council of Hong Kong (614813 and 16212115); Innovation Technology Fund of Hong Kong (No. ITS/273/16FP)

Acknowledgments

The authors would like to thank Prof. J. Xia and his team in Wuhan National Laboratory for Optoelectronics (WNLO) for providing facilities to perform micro-PL measurements, Mr. Chak Wah Tang for his growth assistance, and the NFF and MCPF of HKUST for their technical support.